Academic Journal of Science and Technology
ISSN: 2771-3032 | Vol. 14, No. 3, 2025

Study on FCG of EH36 and EH690 Dissimilar Steel Welded Joints Based on the RA - AF Method of acoustic emission

Yi Zhao, Jian Shi and Xingping Hou

School of Mechanical and Electrical Engineering, Southwest Petroleum University, Chengdu, Sichuan 610500, China

Abstract: This study investigates fatigue crack growth(FCG) in EH36/EH690 dissimilar steel welded joints using acoustic emission (AE) technology. Three specimen types EH36-HAZ, EH690-HAZ, and weld metal(WS) were subjected to fatigue testing under different stress ratios (R=0.1, 0.3 and 0.5) using compact tension (CT) specimens. AE characteristic parameters, including cumulative energy, RA value (Risetime/Amplitude), and AF value (Average Frequency), in conjunction with RA-AF correlation analysis, were employed to elucidate crack propagation mechanisms. The results indicate thatFatigue life of all specimens significantly improves as the R increases, while crack growth rate (da/dN) demonstrates an exponential increase with the rise in stress intensity factor amplitude (ΔK). AE cumulative energy analysis successfully identifies two substages (IIa and IIb) within the stable crack growth phase by detecting variations in the slope. The transition point ΔK decreases with higher R while maintaining material-dependent hierarchy (EH690-HAZ > WS> EH36-HAZ).RA-AF analysis demonstrates a maximum 10% decrease in the proportion of shear cracks as the R increases, suggesting that crack growth is predominantly tensile under high stress conditions. The activation of material defects can lead to a transition from pure tensile fracture modes to mixed tensile-shear fracture modes.

Keywords: Crack propagation; Acoustic emission; RA-AF correlation analysis; Transition point.

1. Introduction

In marine engineering, the reliability of steel structures critically determines the stability and safety of engineering equipment. In numerous engineering scenarios, the performance limitations of single steel grades often prove inadequate for complex operating conditions, thus prompting the development of dissimilar steel welding technology. EH36 high-strength steel, widely used in general engineering structures due to its balanced mechanical properties [1], contrasts with EH690 ultra-high-strength steel, which excels in high-load-bearing applications [2]. Welding these two steels combines their advantages to address diverse engineering requirements. However, dissimilar steel welded joints are prone to fatigue crack formation during service due to compositional and microstructural heterogeneities, posing significant threats to structural integrity [3-4].

Fatigue crack propagation research remains pivotal in engineering reliability. Mechanical components subjected to cyclic loading frequently experience fatigue failure, accounting for over 80% of mechanical part failures [5]. The initiation and progression of fatigue cracks follow a gradual process: microcracks initially evade detection but progressively expand under cyclic loads, ultimately leading to catastrophic fracture and substantial economic losses [6]. Thus, investigating fatigue crack propagation behavior in EH36/EH690 welded joints using acoustic emission (AE) technology holds critical importance for structural safety assurance, maintenance cost reduction, and engineering advancements.

As a nondestructive monitoring technique, AE has been extensively applied across fracture mechanics, materials science, and structural health monitoring [7-11]. Its unique capability to detect microstructural damage makes it particularly valuable for fatigue damage characterization [12-14]. In AE research, characteristic parameters including amplitude, energy, ring-down counts, rise time, and duration are conventionally employed to characterize AE events, serving as critical descriptors that provide direct insights into microstructural alterations within specimens. For instance, K. Du et al. [15] analyzed AE signatures during rock failure modes using Brazilian splitting and shear tests, while Kaizhong Xie et al. [16] correlated AE parameters with bond-slip damage in steel-UHPC interfaces.

Beyond standalone parameter analysis, synergistic use of AE features enables deeper mechanistic insights. Y. Niu et al. [17] employed kernel density estimation to address dataset randomness in RA-AF (Rise time/Amplitude vs. Average Frequency) crack classification. K. Zhao et al. [18] mapped creep-induced fracture modes using RA-AF distributions, and Sizhe Du et al. [19] revealed temperature-dependent shear-to-tensile crack transitions in concrete via RA-AF correlation maps. Hernán Xargay et al. [20] further validated this methodology for assessing thermally treated mortar damage. The RA (Rise time/Amplitude) and AF (Counts/Duration) parameters are widely utilized to investigate fracture modes and damage mechanisms during crack propagation. RA quantifies the relationship between signal rise time and peak amplitude, reflecting the dynamic characteristics and energy features of crack growth. Lower RA values typically correspond to rapid crack propagation (short rise time, high amplitude), while higher RA values indicate slower crack advancement (prolonged rise time). AF represents oscillation frequency per unit time, where high-frequency signals associate with brittle fracture, microcrack acceleration, or localized plasticity, and low-frequency components relate to stable macrocrack growth or friction. Although RA-AF analysis has been predominantly applied to non-metallic materials like concrete and composites [21-23], its use in metallic damage mechanism identification remains limited.

This study provides a methodological reference for RA-AF-based fatigue crack monitoring in metallic systems.

This work systematically investigates fatigue crack propagation in EH36/EH690 welded joints and their HAZ through AE parameter analysis and RA-AF methodology. By monitoring crack evolution under varying stress ratios, we elucidate damage mechanisms governing dissimilar steel joint failures, providing critical insights for structural integrity detection in marine engineering applications.

2. Experimental

2.1. Specimen Design

The test materials comprised EH36 and EH690 steel plates with dimensions of 150 mm×1000 mm×16 mm. Dissimilar steel welded joints were fabricated using gas metal arc welding (GMAW) with a single-sided V-groove configuration (included angle: 60°). TH550 welding wire (diameter: 1.2 mm) served as the filler material. The weld was completed in five passes under controlled interpass temperatures of 150–200℃， with a heat input range of 5.43–10.96 kJ/cm.

Standard compact tension (CT) specimens were machined as shown in Fig. 1(a). Three specimen types were prepared: EH36-HAZ, EH690-HAZ, and WS. Material extraction locations are illustrated in Fig. 1(b).

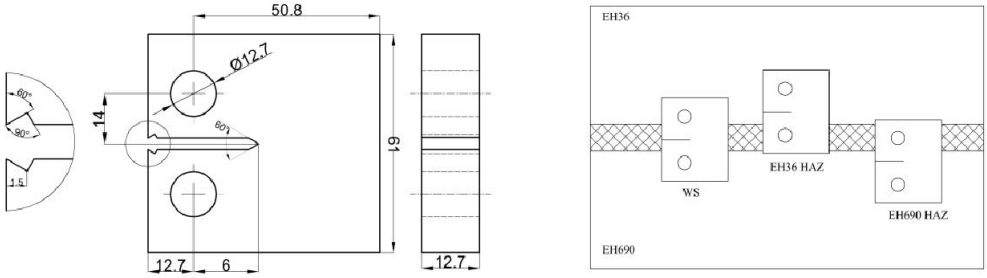

(a)Dimensional schematic of CT specimen (b)Material extraction locations

Figure 1. Specimens

2.2. Experimental Procedure

Fatigue testing was conducted using an MTS809.25 electro-hydraulic servo tension-torsion fatigue testing machine (Fig. 2a). Pre-cracking was performed via the K-decreasing method to achieve a 23 mm initial crack length. The test parameters included a maximum load of 11 kN, stress ratios R = 0.1, 0.3, 0.5, a loading frequency f = 10 Hz, and sinusoidal waveform-controlled loading. Detailed experimental parameters are listed in Table 1.

Table 1. Experimental Parameters

Test Number	Specimens	R	f	F_{max}
C1	EH690-HAZ	0.1	10Hz	11kN
C2	EH690-HAZ	0.3	10Hz	11kN
C3	EH690-HAZ	0.5	10Hz	11kN
C4	EH36-HAZ	0.1	10Hz	11kN
C5	EH36-HAZ	0.3	10Hz	11kN
C6	EH36-HAZ	0.5	10Hz	11kN
C7	WS	0.1	10Hz	11kN
C8	WS	0.3	10Hz	11kN
C9	WS	0.5	10Hz	11kN

The crack propagation process was analyzed following ASTM E647 [24] using the modified seven-point incremental polynomial method to calculate the da/dN-ΔK curve. The stress intensity factor range (ΔK) was determined according to the ASTM-recommended formula:

$$\Delta K = \frac{\Delta P}{B\sqrt{W}} \frac{(2+\alpha)}{(1-\alpha)^{3/2}} (0.886 + 4.64\alpha - 13.32\alpha^2 + 14.72\alpha^3 - 5.6\alpha^4) \quad \text{(eq.1)}$$

$$\alpha = a / W \quad \text{(eq.2)}$$

2.2.1. Where W is the width of the specimen, a is the crack length, ΔP is the change value of the load, and ΔP=Pmax−Pmin

The acoustic emission instrument is the AMSY-6 acoustic emission system produced by Vallen Company in Germany. The model of the AE sensor is VS150-RIC. The amplifier gain is 34 dB, the sampling frequency is 10 MHz, and the threshold value is 34 dB. Vaseline is used as the coupling agent between the sensor and the surface of the specimen, and it is fixed with a magnetic suction buckle to ensure the good reception of the signal, as shown in Fig.2 (b).

(a)MTS testing machine

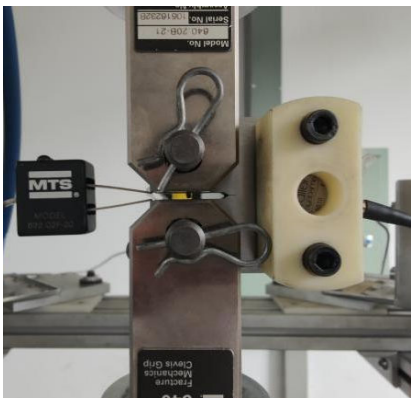

(b) Acoustic emission sensor

Figure 2. The test device

2.3. Principle of RA - AF analysis

2.3.1. Physical mechanism of RA - AF

The core of the RA - AF method lies in the combination of two parameters, AF and RA, to comprehensively analyze the fatigue crack growth. In practical applications, an RA-AF scatter plot is constructed using AF as the vertical axis and RA as the horizontal axis. Distinct regions within the scatter plot correspond to different crack propagation modes and material damage states.

According to a large number of experimental studies and theoretical analyses [25], in the RA - AF plot, when the AF value is high and the RA value is low, it corresponds to the growth of tensile cracks. This is because during the growth of tensile cracks, energy is released instantaneously, generating acoustic emission signals with high frequency and short rise time, thus showing the characteristics of high AF and low RA. Conversely, when the AF value is low and the RA value is high, it corresponds to the growth of shear cracks. During the growth of shear cracks, the internal deformation of the material is relatively complex. The cracks gradually grow along grain boundaries or slip planes, and the energy release is relatively dispersed and slow, resulting in acoustic emission signals with lower frequency and longer rise time. In addition, there may be some transition regions in the RA-AF plot. The scatter points in these regions represent the tensile - shear composite fracture mode, that is, the crack growth process includes both tensile and shear mechanisms. Through the analysis of the RA - AF scatter plot, the growth mode of fatigue cracks at different stages can be intuitively understood, and then the damage evolution process of the material can be further studied, as shown in Fig. 3.

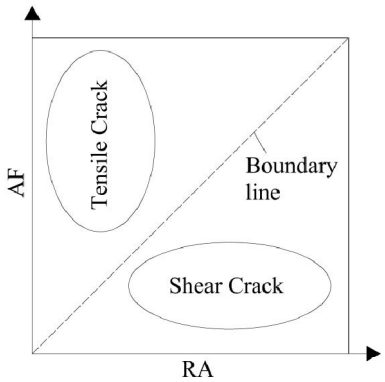

Figure 3. RA-AF Method

2.3.2. Determination of the K value

To accurately determine the slope K of the demarcation line equation AF = K×RA, scholars have explored the proportional relationship between acoustic emission RA and AF. When studying the influence of multi - stage cyclic loading on the classification of fracture modes of marble, Y. Wang et al. [26] proposed that the proportional relationship between the RA value and the AF value is 1:3.75. When analyzing the fracture behavior of concrete during the three - point bending process under different loading rates, X. Q. Fan et al. [27] proposed that the proportional relationship between the RA and AF values is 50:1. Z. H. Zhang et al. [28] compared the crack proportion obtained by introducing the dominant frequency analysis method with the RA - AF method, and the selected K values are: 500 for marble, 400 for fine - grained granite, 350 for diorite, and 150 for coarse - grained granite.

In addition, some scholars introduced intercepts when studying crack classification based on RA and AF values. A. K. Das et al. [29] proposed that the optimal demarcation line for classifying the fracture types of strain - hardening cement - based composite (SHCC) specimens is AF = 26.9841RA - 268.6918. J. S. Li et al. [30] determined that the demarcation line for classifying tensile and shear cracks in siltstone based on the RA and AF values is AF = 93RA + 75.

In summary, the selection of different slope K values can greatly affect the classification effect. In this study, the kneedle algorithm for inflection point monitoring is used to

determine the slope value K of the demarcation line. The Kneedle algorithm for inflection point monitoring determines the most suitable K value for dividing shear cracks and tensile cracks based on the maximum value of the inflection point of the curve of the proportion of shear cracks versus the slope K.

3. Results and Discussion

3.1. FCG Test Results

Table 2. FCG Test Results

Test Number	R	Cycle Number	C	m	R^2
C1	0.1	61287	3.74168×10-9	2.9747	0.96126
C2	0.3	74335	2.24679×10-8	2.5855	0.98295
C3	0.5	175972	2.31848×10-8	2.6110	0.97599
C4	0.1	37502	5.8513×10-9	2.9858	0.97329
C5	0.3	59162	9.8390×10-9	2.8993	0.96333
C6	0.5	134658	9.9514×10-9	2.9727	0.97105
C7	0.1	65950	1.0250×10-9	3.3312	0.98888
C8	0.3	117635	8.7428×10-10	3.4218	0.97448
C9	0.5	195061	5.0106×10-9	3.0752	0.96884

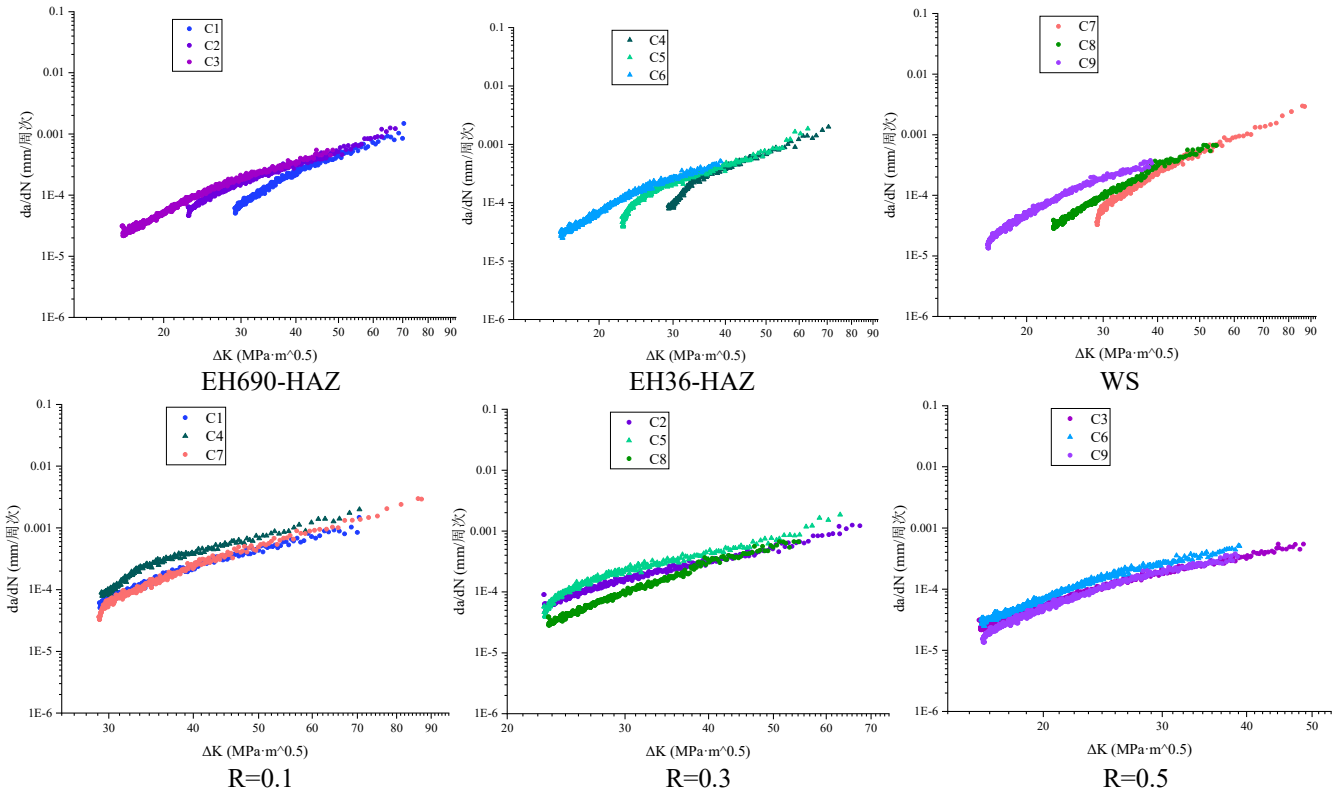

Figure 4. ΔK-da/dN

Table 2 summarizes the number of cycles when the crack length of each specimen ranges from 23 mm to 35 mm, as well as the fitting parameters of the Paris model. It can be seen that all specimens can be well fitted to the Paris model, and the *m* parameters of specimens made of the same material are basically consistent, indicating that the r does not affect the FCGR (Fatigue Crack Growth Rate) curve of the material. With the increase *R* the stress ratio, the fatigue life of the material will also increase, and the fatigue performance of the material has been greatly improved.

Through the fatigue crack growth test, the FCGR curves of different materials and different stress ratios in the double logarithmic coordinate system are obtained, as shown in Fig. 4. The crack growth rates under different stress ratios are in the range of 1×10^{-2} to 1×10^{-6} mm/cycle. Throughout almost the entire fatigue life, the FCGR shows approximately linear behavior with respect to the change of ΔK and follows the Paris law.

When R = 0.1, for the HAZ of EH36, WS, and the HAZ of EH690, at ΔK = 40MPa·m$^{1/2}$, the crack growth rates are 3.52 times, 3.94 times, and 3.73 times respectively compared with those at ΔK = 30MPa·m$^{1/2}$. The crack growth rate shows an exponential upward trend with the increase of ΔK.

3.2. Acoustic Emission Parametric Analysis

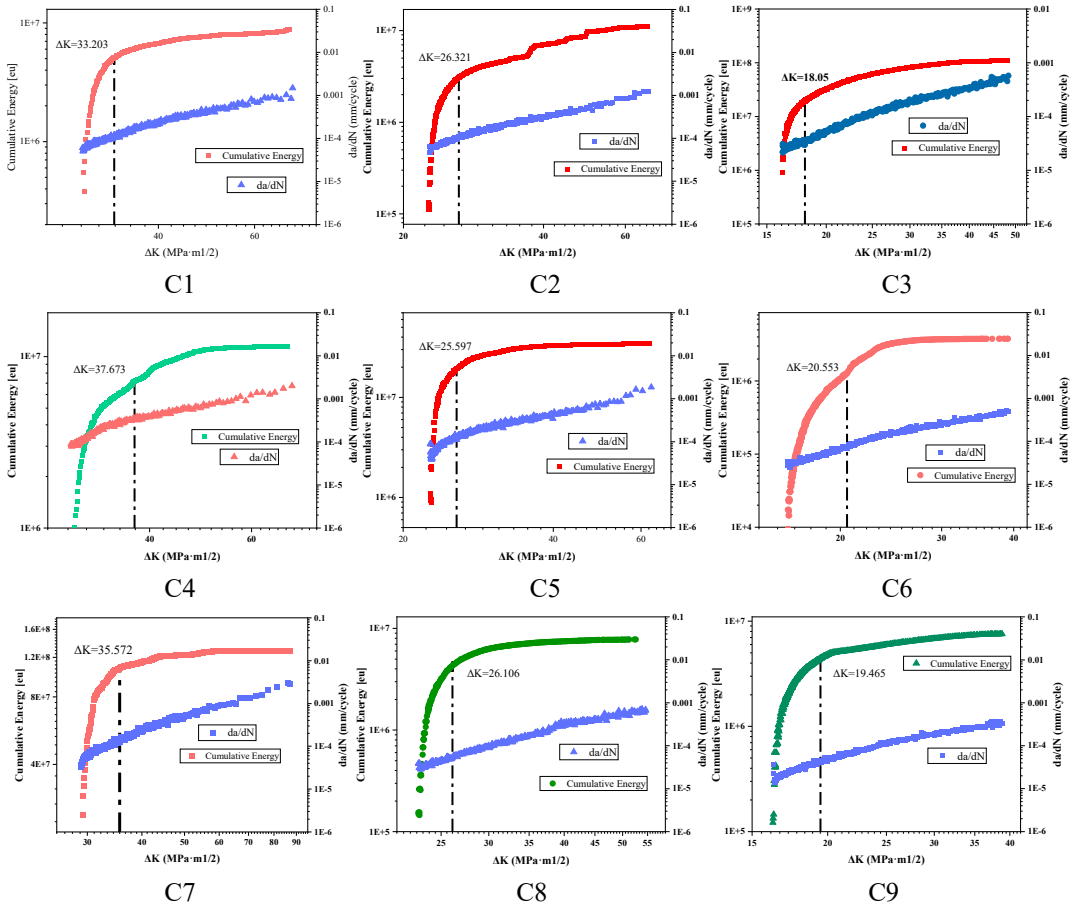

Figure 5. Fatigue crack growth rate, cumulative energy vs. ΔK

Fig. 5 shows the variation in cumulative count and cumulative energy as a function of ΔK for all the specimens. The variation of da/dN vs. ΔK is also included in the plots for comparison. As can be seen from Fig. 5, the slope of the cumulative energy with respect to ΔK changes significantly, clearly indicating the existence of two sub - stages (Stage IIa and Stage IIb) within the stable crack growth stage of the Paris model. Previous studies have reported that in fatigue crack tests, the correlation between da/dN and ΔK in the second stage follows a two-slope behavior [31-34]. The ΔK values at transition from stage IIa to IIb are given in the literature by the following eq.3:

$$\Delta K = \alpha E \sqrt{b} \qquad \text{(eq.3)}$$

where $\alpha = \varepsilon\sqrt{2\pi n 10^6}$, ΔK_0 is the stress intensity factor range at the point of transition in MPa $m^{1/2}$, E is Young's modulus in MPa, b is Burger's vector in m, ε is the ultimate elastic strain in m, $n = r_{cpz} / d$, r_{cpz} is the plastic zone size and d is the grain diameter.

However, in the second stage of crack growth in this study, the two-slope behavior was not observed in the da/dN vs. ΔK curve, but it was clearly shown in the cumulative energy vs. ΔK graph. From the FCGR curve, the transition from Stage IIa to IIb is continuous, and the overlap of these two sub - stages sometimes makes it difficult to distinguish the transition point. Therefore, in this study, the relationship between da/dN and ΔK in the second stage exhibits a single power - law regime. Nevertheless, the existence of the two distinct stages can be clearly recognized through the slope change of the AE cumulative energy with respect to ΔK.

Table 3. Transition points between the two sub-stages

Test Number	R	Experimental Value(MPa·$m^{1/2}$)	Theoretical Value(MPa·$m^{1/2}$)
C1	0.1	33.203	32.798
C2	0.3	26.321	25.221
C3	0.5	18.050	19.352
C4	0.1	37.673	37.392
C5	0.3	25.597	24.679
C6	0.5	20.553	21.068
C7	0.1	35.572	36.012
C8	0.3	26.106	35.750
C9	0.5	19.465	20.113

Table 3 presents the theoretical and experimental transition points between the two sub-stages of the stable crack growth stage in crack propagation , which are derived from the cumulative energy values. Under the same stress ratio, the transition point values of different materials are quite close, and follow the pattern of EH690-HAZ > WS > EH36-HAZ. This indicates that the transition point values are significantly influenced by the stress ratio, while the influence of the material's own properties is minimal. Additionally, it can be observed that as the stress ratio increases, the transition point values of the same material also increase accordingly, suggesting a positive correlation between the change in the stress ratio and the transition point values.

In this section, the identification of sub-stages during the stable crack growth process based on cumulative energy was discussed. The cumulative energy was successfully used to divide the sub - stages of different specimens under different stress ratios, and the correlations between the transition point values, stress ratio, and material characteristics were obtained. In the subsequent research, the RA-AF method will be utilized to further analyze the damage characteristics and mechanisms of the two sub-stages.

3.3. Identification of Damage Characteristics and Mechanisms Based on the RA-AF Method

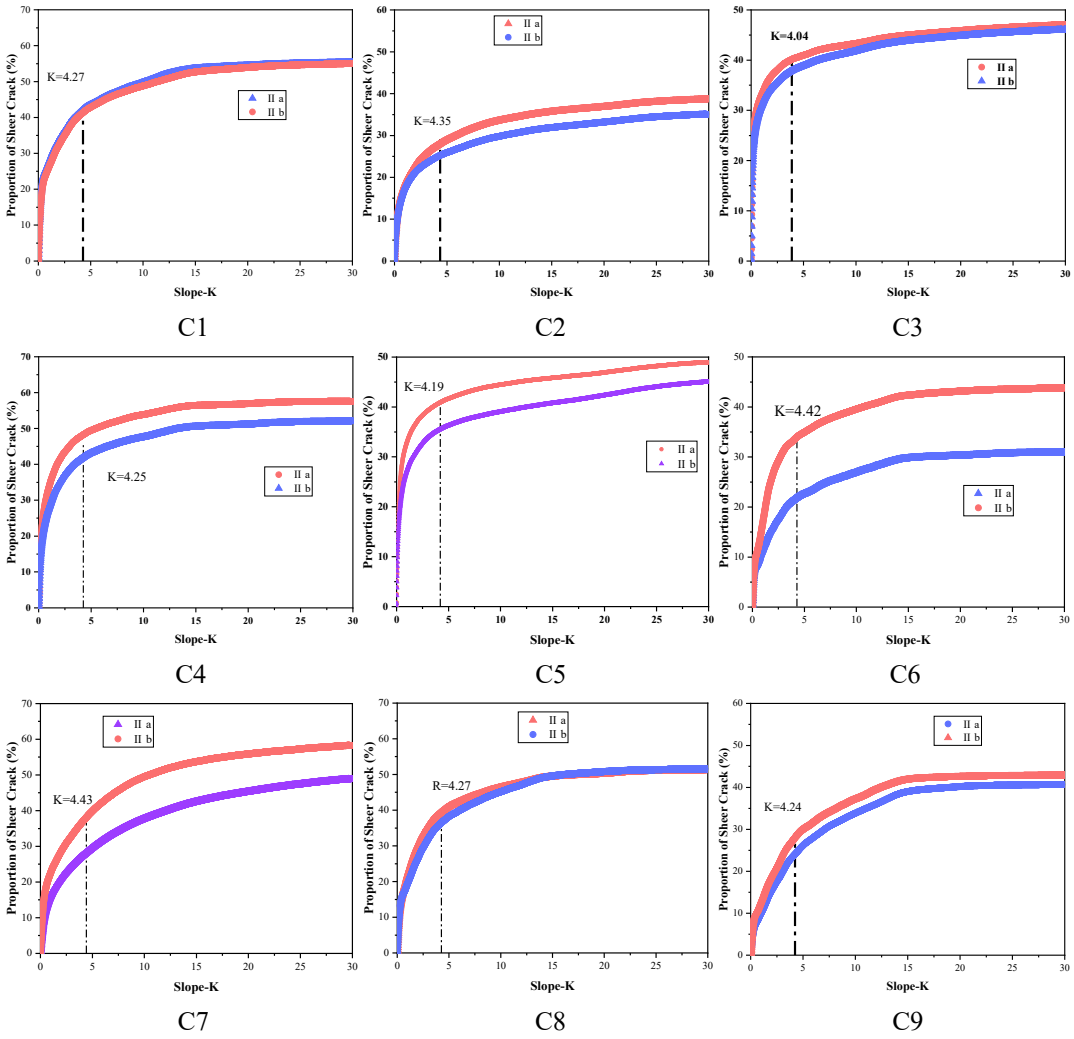

Figure 6. Proportion of Sheer Crack vs. K

Table 4. RA-AF Results

Test Number	R	K	Proportion of Sheer Crack(IIa)%	Proportion of Sheer Crack(IIb)%
C1	0.1	4.27	42.17	41.35
C2	0.3	4.35	28.02	25.23
C3	0.5	4.04	40.29	38.05
C4	0.1	4.25	48.24	41.90
C5	0.3	4.19	40.96	35.60
C6	0.5	4.42	21.77	33.82
C7	0.1	4.43	28.24	38.12
C8	0.3	4.27	39.42	36.46
C9	0.5	4.24	24.28	28.30

Fig.6 shows the variation of the proportion of shear cracks in the two sub - stages during the stable crack growth stage with the slope K.Fig. 4 shows the K value determined by the Kneedle algorithm, as well as the variation in the proportion of shear cracks in the two sub-stages of stable crack growth

From the calculation results, it can be seen that the K-values of most specimens are around 4.30, and the K - values of a small number of specimens decrease slightly to around 4.00. This reflects the unity and accuracy of the demarcation line division in the RA - AF method, and once again proves that it is feasible to conduct damage analysis during the crack growth process through the RA - AF method. Looking at specimens C4 - C6, as the stress ratio increases, the proportion of shear cracks generally decreases, especially from a stress ratio of 0.3 to 0.5, with the largest decrease of about 20%. This indicates that as the stress ratio increases, during the crack growth process of the material, the driving force for crack growth decreases, internal defects of the material are less likely to be induced, tensile cracks always dominate, and the material shows tensile - type failure. For the three specimens with R = 0.5, for specimens C9 and C3 with relatively strong fatigue resistance, the proportion of shear cracks in the two sub - stages changes little. However, for specimen C6, from stage IIb to stage IIa, the proportion of shear cracks increases significantly, and the material damage mode changes from tensile failure to tensile - shear failure. Generally speaking, as the crack growth stage progresses from stage IIa to stage IIb, the proportion of tensile cracks will increase slightly, and tensile cracks further dominate, which indicates that the crack growth process changes towards rapid growth. If there are large internal defects in the material (C6, C9), during the transition to rapid growth, the defects are activated, and the crack growth mode will change from a pure tensile mode to a tensile - shear mixed mode.

4. Conclusion

In this paper, fatigue crack growth experiments were carried out on three different materials (EH36-HAZ, EH690-HAZ, WS) under three grades stress ratios (R = 0.1, 0.3, 0.5), and identification and monitoring were conducted using acoustic emission monitoring counts. Based on the nature of the fatigue process itself, as well as by using acoustic emission characteristic parameters and the RA - AF analysis method, the entire crack growth process was characterized both qualitatively and quantitatively. The crack growth processes under different parameter environments were discussed, and the following conclusions were obtained:

1.Through the basic fatigue crack growth data and acoustic emission characteristic parameters, the crack growth properties of the base metal of EH36, the heat-affected zone, and the weld under different loading conditions were obtained. With the increase of the stress ratio, the crack growth resistance of various materials has been significantly improved.

2.The change points of the cumulative energy count in the load domain (ΔK) can well determine the transition point of the crack stable growth of the dissimilar steel welded joints of EH36 and EH690 from slow crack growth to rapid crack growth, and divide the process into two sub-stages. However, it is impossible to accurately judge in the FCGR curve.

3.In the RA - AF analysis, by using the division of the proportion of shear cracks and tensile cracks, the identification of damage characteristics and mechanisms was successfully completed. It can identify the massive activation of internal defects in the material and determine whether the crack growth mode will change from the tensile mode to the tensile-shear mixed mode.

References

[1] MoLin Su, WenCai Liu, HongQiao Yan, et al. Investigation of tensile, fatigue crack growth behavior and prediction model of EH36 welded joints[J]. Journal of Materials Research and Technology,35,2025,3512-3522.

[2] Xinkang Shen, Xudong Gao, Yongbo Shao, et al. Investigation on the fatigue crack growth behavior of welded joints in EH690 high-strength marine steel[J]. International Journal of Fatigue,189,2024,108572.

[3] VUHERER T, DUNĐER M, MILOVIĆ L, et al. Microstructural investigation of the heat-affected zone of simulated welded joint of P91 steel [J]. Metalurgija, 2013, 52(3).

[4] TAN L, ANDERSON M, TAYLOR D, et al. Corrosion of austenitic and ferritic-martensitic steelsexposed to supercritical carbon dioxide [J]. Corrosion Science, 2011, 53(10).

[5] E. Amsterdam, J.W.E. Wiegman, M. Nawijn, et al. The effect of crack length and maximum stress on the fatigue crack growth rates of engineering alloys[J]. International Journal of Fatigue,161,2022,106919.

[6] Santos D L J I, França E J, Santos M F L, et al. Allocation of performance shaping factors in the risk assessment of an offshore installation[J]. Journal of Loss Prevention in the Process Industries, 2020, 64: 104085-104085.

[7] Sulochana Shrestha, Manigandan Kannan, Gregory N. Morscher, et al. In-situ fatigue life analysis by modal acoustic emission, direct current potential drop and digital image correlation for steel[J]. International Journal of Fatigue, 142, 2021, 105924.

[8] Xianhui Feng, Huilin Liu, Xu Chen, et al. Acoustic emission characteristics and cracking mechanism analysis of anisotropic shale containing a circular hole under uniaxial compression[J]. Theoretical and Applied Fracture Mechanics,135,2025,104771.

[9] Dazhong Zhang, Shiyi Zhang, SM Chayan, et al. Time-frequency characterization of acoustic emission signals from bending damage of corroded reinforced concrete beams in high- temperature saline environment[J]. Case Studies in Construction Materials,22,2025,e04237.

[10] Xing-Yuan Jiang, Di Wu, Zhen-Xian Zhao, et al. Experimental and numerical study on the damage evolution and acoustic emission multi-parameter responses of single flaw sandstone under uniaxial compression,[J]. Theoretical and Applied Fracture Mechanics,133, Part A,2024,104535.

[11] Kai-De Liu, Yu Zhou, Xiao-Ping Zhang, et al. Study on mechanical properties and acoustic emission characteristics of deep diorite under uniaxial compression[J]. Heliyon,10, Issue 2,2024,e24482.

[12] Jingmang Xu, Kai Wang, Qiantao Ma, et al. Study on acoustic emission properties and crack growth rate identification of rail steels under different fatigue loading conditions[J]. International Journal of Fatigue,172,2023,107638.

[13] eza Mohammadi, Mehdi Ahmadi Najafabadi, Hamed Saghafi, et al. The effect of mode II fatigue crack growth rate on the fractographic features of CFRP composite laminates: An

acoustic emission and scanning electron microscopy analysis[J]. Engineering Fracture Mechanics,241,2021,107408.

[14] Bin Xu, Qi Wu. Stress fatigue crack propagation analysis of crane structure based on acoustic emission[J]. Engineering Failure Analysis,109,2020,104206.

[15] DU K,LI X F,TAO M, et al. Experimental study on acoustic emission (AE) characteristics and crack classification during rock fracture in several basic lab tests[J]. International Journal of Rock Mechanics and Mining Sciences,2020,133:104411.

[16] Kaizhong Xie, Kang Huang, Quanguo Wang, et al. Study of bond-slip performance of steel tube with UHPC based on acoustic emission parameter analysis[J]. Structures,70,2024,107828.

[17] NIU Y,ZHOU X P,BERTO F. Evaluation of fracture mode classification in flawed red sandstone under uniaxial compression[J]. Theoretical and Applied Fracture Mechanics, 2020, 107: 102528.

[18] ZHAO K,MA H L,YANG C, et al. The role of prior creep duration on the acoustic emission characteristics of rock salt under cyclic loading[J]. International Journal of Rock Mechanics and Mining Sciences,2022,157:105166.

[19] Sizhe Du, Bo Liang, Yu Zhang, et al. Mechanical properties and damage characteristics analysis on recycled aggregate concrete with glazed hollow beads after high temperatures by acoustic emission method[J]. Journal of Building Engineering, 90, 2024, 109429.

[20] Hernán Xargay, Alejandra Vesga-Ramírez, Marianela Ripani, et al. Acoustic Emission monitoring of OPC mortars at elevated temperatures in fracture tests[J]. Procedia Structural Integrity,64,2024,1790-1797.

[21] L.R. Botvina, A.I. Bolotnikov, I.O. Sinev, et al. Acoustic emission, damage and fracture mechanisms of structural steel under mixed-mode loading [J]. Engineering Fracture Mechanics, 292,2023,109635.

[22] Suresh Nuthalapati, K.E. Kee, Mokhtar B. Che Ismail, et al. Detection and characterization of chloride induced stress corrosion cracking on SS304 under thermal insulation using acoustic emission technique[J]. Engineering Failure Analysis, 168, 2025,109094.

[23] Hui Wei, Baosheng Xu, Jue Li, et al. Effect of temperature on fatigue damage evolution of asphalt mixture based on cluster analysis and acoustic emission parameters[J]. Engineering Fracture Mechanics,Volume 317,2025,110954.

[24] ASTM E647.Standard test method for measurement of fatigue crack growth rates[S]. Annual book of ASTM standards,2010. Philadelphia.

[25] Monitoring method for active cracks in concrete by acoustic emission:JCMS-III B5706[S]. Japan:Federation of Construction Materials Industries,2003.

[26] WANG Y,ZHANG B,GAO S H,et al. Investigation on the effect of freeze-thaw on fracture mode classification in marble subjected to multi-level cyclic loads[J]. Theoretical and Applied Fracture Mechanics,2021,111:102847.

[27] FAN X Q,LI S T,CHEN X D,et al. Fracture behaviour analysis of the full-graded concrete based on digital image correlation and acoustic emission technique[J]. Fatigue and Fracture of Engineering Materials and Structures,2020,43:1 274–1 289.

[28] ZHANG Z H,DENG J H. A new method for determining the crack classification criterion in acoustic emission parameter analysis[J]. International Journal of Rock Mechanics and Mining Sciences,2020,130:104323.

[29] DAS A K,SUTHAR D,LEUNG C K Y. Machine learning based crack mode classification from unlabeled acoustic emission waveform features[J]. Cement and Concrete Research,2019,121:42–57.

[30] LI J S,LIAN S L,HUANG Y S,et al. Study on crack classification criterion and failure evaluation index of red sandstone based on acoustic emission parameter analysis[J]. Sustainability,2022,14(9):5 143.

[31] Chan KS. Scaling laws for fatigue crack growth of large cracks in steels[J]. Metal Trans A 1993;24:2473–86.

[32] Chan KS, Pan YM, Davidson D, Mcclung RC. Fatigue crack growth mechanisms in HSLA-80 steels[J]. Mater Sci Eng A 1997;222:1–8

[33] Kumar J, Ahmad S, Mukhopadhyay CK, Jayakumar T, Kumar V. Acoustic emission studies for characterization of fatigue crack growth behavior in HSLA steel[J]. Nondestr Test Eval 2016;31:77–96

[34] Amsterdam E, Grooteman F. The influence of stress state on the exponent in the power law equation of fatigue crack growth[J]. Int J Fatigue 2016;82:572–8.